# Role of the lever arm in the processive stepping of myosin V

**Thomas J. Purcell*, Carl Morris†, James A. Spudich*‡, and H. Lee Sweeney†**

*Department of Biochemistry, Stanford University Medical Center, Stanford, CA 94305; and †Department of Physiology, University of Pennsylvania School of Medicine, Philadelphia, PA 19104

Contributed by James A. Spudich, September 4, 2002

**Myosin V is a two-headed molecular motor that binds six light chains per heavy chain, which creates unusually long lever arms. This motor moves processively along its actin track in discrete 36-nm steps. Our model is that one head of the two-headed myosin V tightly binds to actin and swings its long lever arm through a large angle, providing a stroke. We created single-headed constructs with different-size lever arms and show that stroke size is proportional to lever arm length. In a two-headed molecule, the stroke provides the directional bias, after which the unbound head diffuses to find its binding site, 36 nm forward. Our two-headed construct with all six light chains per head reconstitutes the 36-nm processive step seen in tissue-purified myosin V. Two-headed myosin V molecules with only four light chains per head are still processive, but their step size is reduced to 24 nm. A further reduction in the length of the lever arms to one light chain per head results in a motor that is unable to walk processively. This motor produces single small ≈6-nm strokes, and ATPase and pyrene actin quench measurements show that only one of the heads of this dimer rapidly binds to actin for a given binding event. These data show that for myosin V with its normal proximal tail domain, both heads and a long lever arm are required for large, processive steps.**

Myosin V is an actin-based motor (1) that has been implicated in several forms of organelle transport (2). It is a two-headed motor. Each head consists of a catalytic domain, which contains the ATPase and actin-binding activities, followed by an extended domain with six light-chain binding sites (IQ repeats). The light-chain binding domain is also referred to as the lever arm (3–5). The two heads are held together by the proximal tail, which is a coiled coil. The remaining distal tail is a putative cargo binding domain (6). Unlike muscle myosin II, which depends on large arrays for function, myosin V can move cargo as a single molecule by processively stepping along actin (7). Processivity means that one molecule can undergo multiple productive catalytic cycles and associated mechanical steps before it detaches from its track. Single-molecule analysis reveals that each catalytic cycle consists of a discrete displacement followed by an ADP release limited dwell (8). Multiple cycles produce staircases in single-molecule traces.

To understand the mechanism for chemomechanical transduction, one must decipher the roles of the various domains of the molecule. Evidence shows that myosins function by swinging the extended lever-arm domain, whereas the catalytic domain is bound to actin (3–5). As described above, myosin V has a large lever arm, consisting of six light-chain binding domains. Single molecules of native myosin V and a truncated heavy meromyosin (HMM) version expressed in baculovirus take ≈36-nm steps and move processively along actin (7–10). We hypothesize that myosin V is able to take processive 36-nm steps by walking along the actin filament hand over hand. Myosin V has been shown by electron microscopy to span a 36-nm pseudorepeat of the actin filament (11). The 36-nm step consists of an ≈20-nm power stroke; the remainder of the step comes from a diffusive search (10, 12). A nucleotide-dependent conformational change in the protein swings the lever arm, producing the power stroke.

Recently, Tanaka *et al*. (13) constructed a chimeric molecule consisting of the myosin V catalytic domain, a single IQ repeat of the light-chain binding domain, and a portion of smooth muscle myosin rod. They report that this chimera produced staircases with ≈30-nm steps. Because this size is close to the value for a myosin V with a full 6IQ lever arm, they concluded that the large step size requires only the catalytic domain and that native myosin V does not use a swinging lever arm to generate a large step in motion. They argue that the motion is completely driven by Brownian motion of the myosin that is captured by the polar actin filament.

In the present study we further explore the role of the light-chain binding domain of myosin V as a lever arm to produce large steps along actin. We use a simplified surface attachment and a laser trap to measure the step sizes and processivity of single- and double-headed myosin V with either a WT lever arm with 6IQ repeats or a shortened lever arm with either 4IQ repeats or a single IQ repeat. The surface attachment consists of monoclonal anti-GFP bound to the surface. This antibody links to GFP fused at the C terminus of a myosin V that has been truncated to form a HMM-like molecule. By analogy to myosin II, HMM consists of the motor domain and a sufficient amount of the coiled-coil tail domain to ensure dimerization. The 4IQ construct was generated by deletion of the fifth and sixth IQ motifs from the myosin V-6IQ-HMM. Similarly, the 1IQ construct was generated by deletion of the second through sixth IQ motifs. Thus, the normal proximal myosin V tail is present in all of the two-headed species examined. Single-headed species were made by removing the coiled coil and directly fusing the motor domain to GFP.

## Materials and Methods

**Baculovirus Expression of Constructs.** Chicken myosin V cDNA was expressed in six forms (Fig. 1*A*). The constructs were based on the previously described two-headed (HMM-like) myosin construct, myosin V-6IQ-HMM (9). The construct was used to create a recombinant baculovirus used for coexpression in SF9 cells with calmodulin and essential light chains (9). By using the methodology detailed by Sweeney *et al.* (14), purified myosin V protein was obtained. This myosin V-6IQ-HMM heavy chain was truncated at Glu-1099. A leucine zipper (GCN4) was added after the native myosin coiled coil to ensure dimerization, followed by enhanced GFP and a FLAG tag to facilitate purification. Myosin V-4IQ-HMM and myosin V-1IQ-HMM constructs were made in the same manner, except either two or five of the six IQ motifs were removed, respectively. For the myosin V-4IQ-HMM, the heavy chain was truncated at Arg-863 and joined to heavy-chain residue Ile-911, thus removing IQ motifs 5 and 6. For myosin V-1IQ-HMM, the heavy chain was truncated at Arg-791 and joined to heavy-chain residue Ile-911, thus removing IQ motifs 2–6.

For the single-headed (S1-like) constructs, the coiled coil was removed and a 15-aa linker preceded the GFP-Flag. The linker

Abbreviation: HMM, heavy meromyosin.

‡To whom correspondence should be addressed. E-mail: jspudich@cmgm.stanford.edu.

BIOPHYSICS

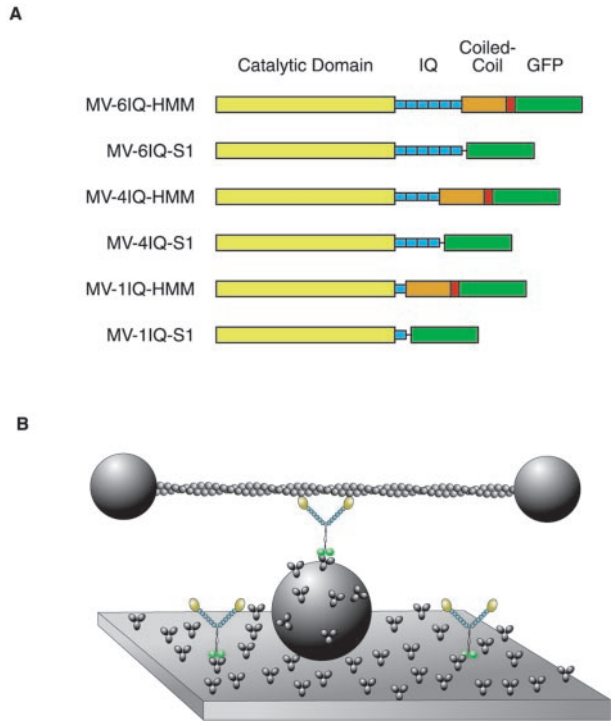


**Fig. 1.** Diagram of constructs and experimental trap setup. (*A*) Diagrams of constructs. The myosin V head consists of the catalytic domain (yellow) and the light-chain binding IQ repeats (blue). The two-headed HMM constructs have a tail domain that contains native myosin V coiled coil (orange) with a short segment of GCN4 (red) to ensure dimerization. All constructs have GFP (green) and a FLAG tag (not shown) at the C terminus. (*B*) Experimental setup for recording single myosin molecules. An actin filament, stretched between two trapped polystyrene beads, is brought into contact with myosin molecules adsorbed onto the surface by anti-GFP antibodies.

sequence (GEQKLISEERMRRGG) was added after heavy-chain amino acid Arg-791 to create myosin V-1IQ-S1, after Arg-863 to create myosin V-4IQ-S1, and after Lys-910 to create myosin V-61Q-S1. Recombinant baculoviruses were generated, and expression and purification was as for the HMM species.

All constructs produced smooth, continuous movement in *in vitro* motility assays, indicating very few inactivated heads.

**Flow Cell Preparation.** All trap and *in vitro* motility assays were performed in flow cells prepared as described (9). Assay buffer included 25 mM imidazole HCl (pH 7.4), 25 mM KCl, 5 $\mu$M calmodulin, 1 mM EGTA, 10 mM DTT, and 4 mM $MgCl_2$; an oxygen-scavenging system to retard photobleaching (25 $\mu g \cdot ml^{-1}$ glucose oxidase, 45 $\mu g \cdot ml^{-1}$ catalase, and 1% glucose); and an ATP regeneration system (0.1 $mg \cdot ml^{-1}$ creatine phosphokinase, 1 mM creatine phosphate). *In vitro* motility and trap assays on processive staircases were performed in 2 mM ATP. Single-stepping nonprocessive trap assays used 0.5–20 $\mu$M ATP.

Motors were adsorbed to a nitrocellulose coverslip by a specific surface attachment with monoclonal anti-GFP antibody (3E6, Qbiogene). After treatment with antibody (0.05 mg/ml), the surface was blocked by additional treatment with 1 mg/ml BSA. Dilutions of motor were then flown into the cell.

**Optical Trap.** Optical trap assays were performed as described (9, 15). For nonfeedback experiments the actin was stretched taut; that is, stretched until moving one bead with the laser beam pulled the other bead approximately the same distance.

Biotinylated actin filaments were stretched between two trapped 1-$\mu$m-diameter polystyrene beads coated with streptavidin to form a dumbbell. Actin dumbbells were brought into contact with myosin adsorbed to 1.5-$\mu$m glass beads that were tightly adhered to the surface of the flow cell.

Processive steps were identified by eye and calculated as the difference in mean position before and after the step. For nonprocessive motors, binding events were selected by two

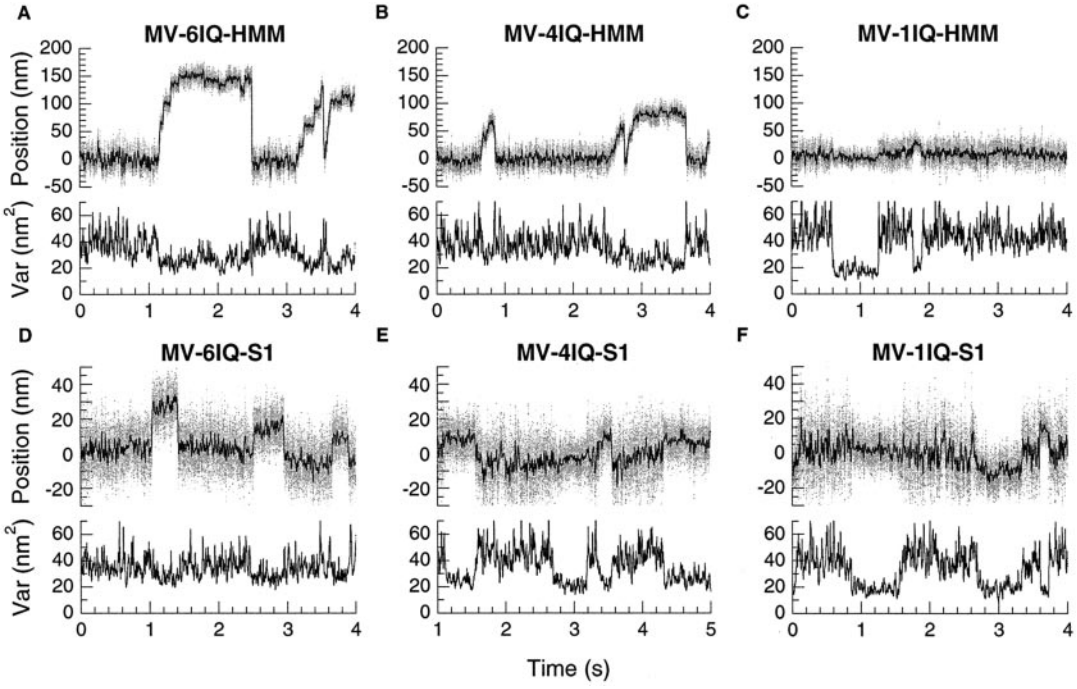


**Fig. 2.** Sample data from trap. Bead position is shown in the upper trace in each graph, and variance is shown below. Variance, which is inversely proportional to the net stiffness of all attachments to the bead, is calculated over a 1-ms window. Decreases in variance correspond to the increased stiffness of the system due to actin binding to a motor on the surface. One source of the apparent wide distribution of single-step sizes is caused by randomness in the starting position of the actin filament due to Brownian motion before myosin binding (16).

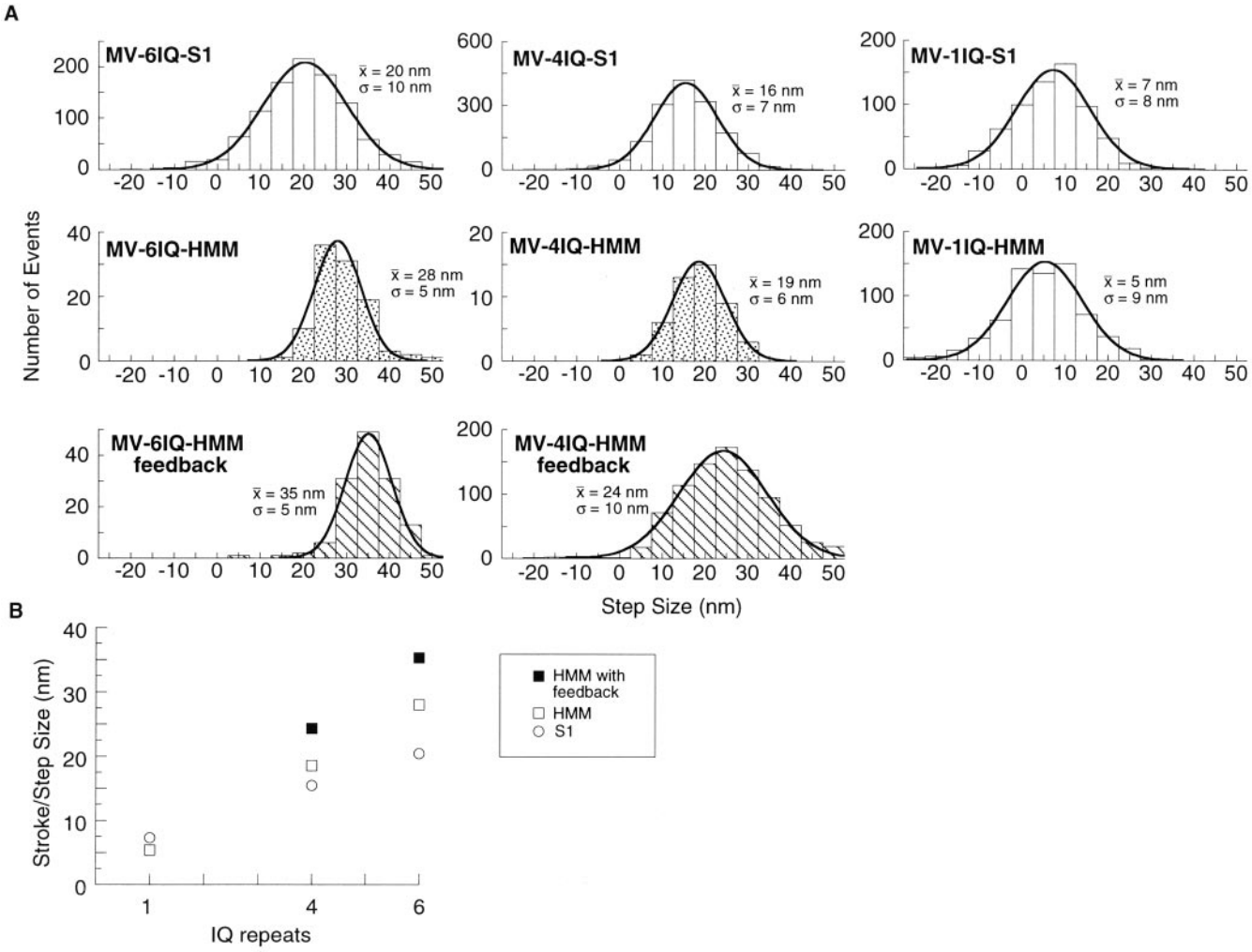


**Fig. 3.** Effect of lever arm length on step size. (*A*) Step size histograms. Comparison of step sizes for the various constructs, pooled from several experiments. The mean ($\bar{x}$) and standard deviation ($\sigma$) were obtained by a least-squares fit of each histogram to a Gaussian distribution. Molecules that produce only a single step are shown with plain bars. Histograms for MV-6IQ-HMM and MV-4IQ-HMM represent step sizes in processive staircases. Stippled histograms represent the step size of the motor stepping against a stationary trap. Striped histograms represent stepping against constant 1 pN of backward force, by using a feedback-controlled trap (8, 9). (*B*) Step size is proportional to lever arm length. The mean of each histogram from *A* is plotted against lever arm length, showing the dependence of step size on lever arm length.

methods. One method involved identification of drops in the variance of bead position that arises from increased stiffness due to surface attachment (Fig. 2) (16). The second method involved identification of drops in the bead–bead correlation of Brownian motion due to mechanical isolation of the two beads (17). Stroke size was calculated as the difference between mean bead displacement during the binding event and mean bead location 0.1 s before and after the event. Stroke size results were pooled from 4–9 separate experiments to control for systematic variation in the availability of myosin binding sites on the suspended actin filament (18). The ATP concentration was lowered to 0.5–20 $\mu$M to extend binding events, making them easier to identify.

**Actin-Activated ATPase Measurements.** The actin-activated Mg-ATPase activity of the 1IQ myosin constructs was determined by using the NADH-coupled assay in a spectrophotometer by monitoring the absorbance change at 340 nm. The ATPase solution was composed of 10 mM imidazole (pH 7.0), 50 mM KCl, 1 mM $MgCl_2$, and 1 mM $K^+$-EGTA (KMg50) with 200 $\mu$M NADH, 250 $\mu$M phospho*enol*pyruvate, 10 units/ml lactate dehydrogenase, and 50 units/ml pyruvate kinase, and it included 0.025–0.1 $\mu$M myosin V. The solutions also contained 0–30 $\mu$M F-actin and 5 $\mu$M calmodulin. The reaction was initiated by addition of 2 mM MgATP. The assays were performed at 25°C.

**Transient Kinetics.** Kinetic measurements were performed as described (19) at 25°C by using an Applied Photophysics SX.18MV Stopped-Flow Spectrometer (Surrey, U.K.). Pyrene actin, prepared as described (20), was excited at 365 nm and the fluorescence measured by using a 400-nm long-pass filter. The rate of myosin V binding to actin was determined in KMg50 buffer and included 250 $\mu$M MgADP.

## Results

We made the constructs shown in Fig. 1*A* to test the effect of lever arm length on the step size that myosin V can produce. We used the dual-beam laser trap method (21, 22) (Fig. 1*B*) to measure the step size of single molecules. The myosin concentration was adjusted until 5–30% of the platforms tested showed myosin activity. MV-6IQ-HMM behaved like WT tissue-purified myosin V (7) (Fig. 2*A*). After binding to the actin dumbbell, the MV-6IQ-HMM took several discrete steps producing a staircase.

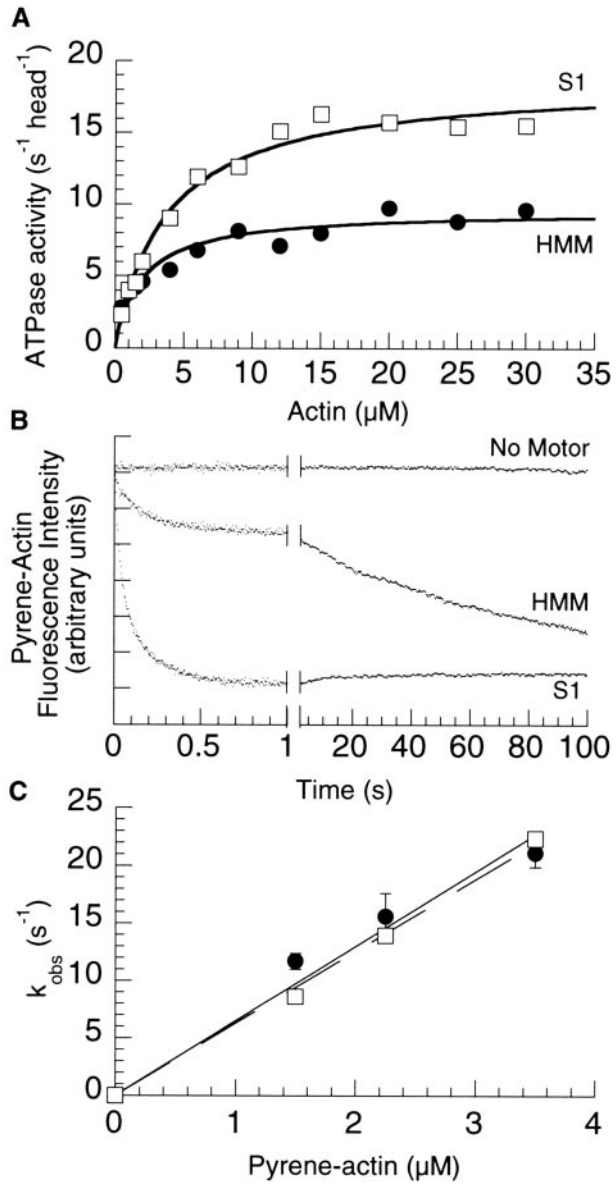


**Fig. 4.** One head is excluded in the myosin V-1IQ-HMM. (*A*) Actin-activated ATPase. The ATPase activity per head of the two-headed HMM (●) is approximately half that of the single-headed S1 (□). (*B*) Time course of pyrene quenching after mixing 2.25 μM pyrene actin with KMg50 (*Top*), 0.2 μM heads 1IQ-HMM (*Middle*), or 0.2 μM heads 1IQ-S1 (*Bottom*). The time axis has been split to show both the fast and slow phase of pyrene quenching in the HMM construct. (*C*) Actin concentration dependence of the fast rate of binding of MV-1IQ-HMM and MV-1IQ-S1. The fast phase binding rate of the myosin V constructs was measured at pyrene actin concentrations from 1.5 to 3.5 μM at 25°C in KMg50 buffer with 250 μM MgADP added. The fast phase rates of the HMM (●) and S1 (□) plotted against actin concentration was fit by using linear regressions passing through the origin with the slope describing the apparent second-order binding constant.

The motor took three or four steps until the motor stalled against the force of the stationary trap. Single molecules of MV-4IQ-HMM also produced staircases on binding to actin (Fig. 2*B*). In a stationary trap, the amplitude of each bead displacement for the 4IQ motor averaged 19 nm, compared with 28 nm for MV-6IQ-HMM (Fig. 3). These values are an underestimate of the true step size because each step results in greater backward force, stretching out compliant elements in the motor and actin-bead dumbbell. To measure the true step of each motor quantitatively, the backward force was held constant at 1 pN by using a feedback-controlled trap (9). Under these conditions, the MV-6IQ-HMM produced a mean 35-nm step, whereas the MV-4IQ-HMM averaged 24 nm (Fig. 3).

MV-1IQ-HMM did not produce staircases, indicating that this construct does not show processive movement. Essentially all binding events consisted of a single stroke followed by dissociation of the motor (Fig. 2*C*). The lack of staircases was also observed for all of the single-headed constructs (Fig. 2 *D–F*). The amplitude of strokes for MV-1IQ-HMM was very close to the single-headed MV-1IQ-S1 construct (5 and 7 nm, respectively). MV-4IQ-S1 produced a larger, 16-nm stroke, and MV-6IQ-S1 had a 20-nm stroke. This value for myosin V S1 with all six IQ repeats is very close to a previously reported value of 19 nm (10).

**ATPase and Pyrene Quench Measurements Reveal Half-Site Reactivity.** The inability of the two-headed 1-IQ motif myosin V construct to move processively and the similarity in its stroke size to that of the single-headed 1-IQ motif construct suggested that one of the two heads in this two-headed construct may be blocked. We therefore tested it for half-site reactivity by using actin-activated ATPase (Fig. 4*A*). The single-headed MV-1IQ-S1 hydrolyzed ATP at 18.6 $s^{-1}$ per head ($K_m$ = 3.9 μM actin), whereas the two-headed MV-1IQ-HMM hydrolyzed ATP at 9.5 $s^{-1}$ per head ($K_m$ = 2.0 μM actin), indicating only one head of the MV-1IQ-HMM is active at any one moment.

To determine directly whether one or both heads of the two-headed 1-IQ myosin V construct bound to actin, we measured the rate of myosin V binding to pyrene-labeled actin. The initial rate of pyrene actin quenching was measured after mixing with either the one-headed myosin V 1-IQ or the two-headed myosin V 1-IQ (Fig. 4*C*). The apparent second-order rate constant for both constructs was similar, $6.5 \times 10^6$ $M^{-1}{\cdot}s^{-1}$ for the two-headed construct and $6.3 \times 10^6$ $M^{-1}{\cdot}s^{-1}$ for the one-headed construct. However, the amplitude of the initial quenching for the two-headed construct (on a per-head basis) was approximately half that of the one-headed construct. Furthermore, examination of the traces for the two-headed construct revealed an additional slow quench in the pyrene fluorescence (Fig. 4*B*), which was observed only with the two-headed construct, at all actin concentrations, with an actin-independent rate of 0.015 ± 0.003 $s^{-1}$, suggesting asymmetric binding of two heads. The amplitudes of the fast and slow fluorescence changes were similar, indicating that once the first head binds, the second head's binding is inhibited by steric constraints and binds to the actin more slowly.

## Discussion

Myosin V processive stepping consists of discrete 36-nm displacements. Our experiments seek to test the importance of the lever arm for those steps and determine the mechanism of stepping. Myosin V has an extended light-chain binding domain compared with myosin II. One model is that the molecule swings this domain as a lever and therefore positions the unbound head over the next actin-binding site. Tanaka *et al.* (13) propose a lever arm-independent model in which the motor domain slides along the actin filament, resulting in a 36-nm step.

Our data strongly support the model that the lever arm is critical for the 36-nm step of myosin V. Our 6IQ-HMM construct reconstitutes the activity of the native motor purified from tissue. A myosin V with only four light-chain binding motifs steps processively with a 24-nm step, which is proportional to the reduction in the length of the lever arm. Furthermore, the myosin V with only one light-chain binding motif abolishes processive movement and further reduces the apparent step size (stroke) to ≈6 nm. Thus, a correlation exists between lever arm length and step size.

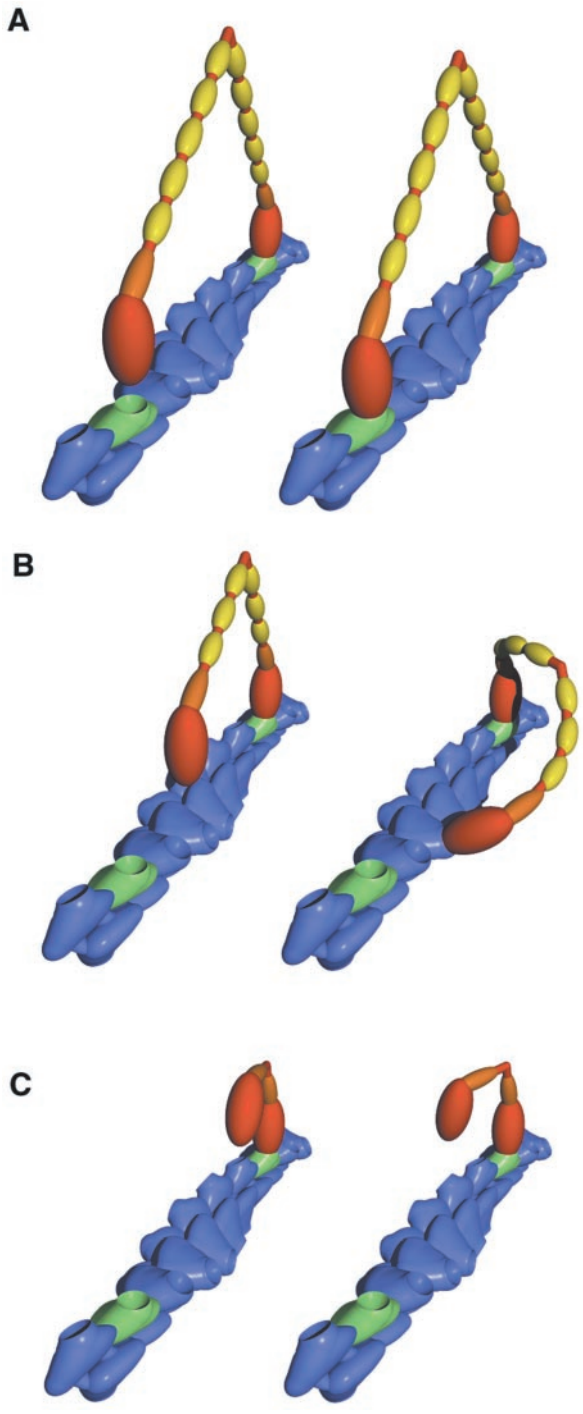


**Fig. 5.** Model of myosin V stepping. A short segment of an actin filament is shown in blue, with the 36-nm pseudorepeat highlighted by green subunits. Each actin subunit has a single myosin binding site depicted as a pit. Each myosin is colored to show the heavy chain including the catalytic domain (red), the essential light chain (orange), and the calmodulin light chains (yellow). (*A*) The rear head of a 6IQ-HMM in a poststroke state, tightly bound to an actin subunit (*Left*). The near head is not yet bound, but in its diffusional search it can easily bind to the green monomer (*Right*). (*B*) The smaller stroke of the bound head of the 4IQ-HMM is shown (*Left*). The unbound head is not positioned so that a binding site is immediately available. The geometry of the actin filament dictates that some portion of the myosin molecule must distort to bind both heads at once. It is possible that the lever arm elastically bends to achieve this conformation (*Right*). (*C*) The 1IQ-HMM is shown bound by one head to an actin filament. The second head can bind only if considerable distortion exists in the myosin. These extreme conformations are likely to be rare, accounting for the fact that the second head binds to actin many orders of magnitude slower than the first head.

This correlation also is seen in the stroke size of the single-headed constructs. For the 6IQ-S1, the stroke was 20 nm, whereas it was 16 nm for the 4IQ-S1 and 7 nm for the 1IQ-S1. Thus, the stroke size clearly decreases as lever arm length decreases.

Our data are consistent with the following model for native myosin V stepping. The step begins with a head in a prestroke state tightly binding actin at a specific site. This tightly bound head then undergoes a conformational change (stroke) with the lever arm swinging to a poststroke state. This conformational change swings the unbound, rear head forward, allowing it to bind to a site on the actin filament that is 36 nm in front of the first head.

The reduced length of the 4IQ lever arm results in a reduced step size. Note that the distribution of step sizes in the histogram in Fig. 3 is broader for the 4IQ-HMM than the 6IQ-HMM construct under constant force in the feedback-controlled trap. The structure of the myosin V molecule is likely to have evolved to bring the unbound head into contact with a binding site on actin that has the same azimuthal orientation as that of the tightly bound head (Fig. 5*A*), which allows the myosin V to efficiently and accurately follow the 36-nm pseudorepeat of actin, generating highly reproducible steps. Although it is processive, the MV-4IQ-HMM is forced to rotate about the axis of the actin filament to find an available actin-binding site (Fig. 5*B*). This unnatural constraint may result in a wider range of step sizes.

It is not surprising that the MV-1IQ-HMM motor does not produce staircases under single-molecule conditions. Simultaneous binding of two heads is essential for a hand-over-hand lever arm model, and the structural constraints of this construct make it unlikely that both heads can easily bind (Fig. 5*C*). Indeed, our data show that the second head of the MV-1IQ-HMM is unable to bind rapidly to the actin. This structural constraint probably lies in the connection between the catalytic domain (red, Fig. 5) and the first light-chain-bound IQ motif (orange, Fig. 5). It seems plausible that the movement of the first light-chain domain relative to the catalytic domain has evolved to swing through an arc that is parallel to the long axis of the actin filament and gives the motor directionality as it swings from its prestroke state to its poststroke state. This constraint prevents the 1IQ from finding a binding site that is outside the plane of this rotation. The additional light-chain binding domains in the 4IQ construct (Fig. 5*C*) provide the necessary flexibility for the second head to find its site.

In contrast to our results, Tanaka *et al.* (13) observed large steps from a two-headed myosin V with a single IQ repeat per head. Their construct was a fusion of the myosin V motor domain with one IQ repeat to a portion of the smooth muscle myosin rod. Their large steps were in the context of a much wider distribution of step sizes than observed with native myosin V. It is possible that compliant elements somewhere in their chimeric construct allow what would be a naturally smaller step size to be augmented by a large diffusional search, producing their observed wide distribution of steps, including large steps.

All of the two-headed constructs reported here were created by simply selectively removing light-chain binding domains from the myosin V, leaving the catalytic and proximal tail dimerization domains intact. Consistent with the lever arm hypothesis, these constructs produced step sizes that are proportional to lever arm length. In summary, our results strongly support the hypothesis that the lever arm plays a significant role in the large, processive step of native myosin V.

We thank C. Baldacchino and J. Nolt, who made and purified the protein, and L. Chen, who assisted in the construction of the constructs. We also thank R. Rock, S. Rice, D. Altman, S. Churchman, and Z. Oekten for their comments on the manuscript. T.J.P. is supported by National Institutes of Health Training Grant GM07276. H.L.S. is supported by National Institutes of Health Grant AR-35661. J.A.S. is supported by National Institutes of Health Grant GM 33289.

1. Cheney, R. E., O'Shea, M. K., Heuser, J. E., Coelho, M. V., Wolenski, J. S., Espreafico, E. M., Forscher, P., Larson, R. E. & Mooseker, M. S. (1993) *Cell* **75,** 13–23.
2. Reck-Peterson, S. L., Novick, P. J. & Mooseker, M. S. (1999) *Mol. Biol. Cell* **10,** 1001–1017.
3. Spudich, J. A. (2001) *Nat. Rev. Mol. Cell. Biol.* **2,** 387–392.
4. Tyska, M. J. & Warshaw, D. M. (2002) *Cell Motil. Cytoskeleton* **51,** 1–15.
5. Geeves, M. A. & Holmes, K. C. (1999) *Annu. Rev. Biochem.* **68,** 687–728.
6. Wu, X., Wang, F., Rao, K., Sellers, J. R. & Hammer, J. A., III (2002) *Mol. Biol. Cell* **13,** 1735–1749.
7. Mehta, A. D., Rock, R. S., Rief, M., Spudich, J. A., Mooseker, M. S. & Cheney, R. E. (1999) *Nature* **400,** 590–593.
8. Rief, M., Rock, R. S., Mehta, A. D., Mooseker, M. S., Cheney, R. E. & Spudich, J. A. (2000) *Proc. Natl. Acad. Sci. USA* **97,** 9482–9486.
9. Rock, R. S., Rice, S. E., Wells, A. L., Purcell, T. J., Spudich, J. A. & Sweeney, H. L. (2001) *Proc. Natl. Acad. Sci. USA* **98,** 13655–13659.
10. Veigel, C., Wang, F., Bartoo, M. L., Sellers, J. R. & Molloy, J. E. (2002) *Nat. Cell Biol.* **4,** 59–65.
11. Walker, M. L., Burgess, S. A., Sellers, J. R., Wang, F., Hammer, J. A., III, Trinick, J. & Knight, P. J. (2000) *Nature* **405,** 804–807.
12. Moore, J. R., Krementsova, E. B., Trybus, K. M. & Warshaw, D. M. (2001) *J. Cell Biol.* **155,** 625–635.
13. Tanaka, H., Homma, K., Iwane, A. H., Katayama, E., Ikebe, R., Saito, J., Yanagida, T. & Ikebe, M. (2002) *Nature* **415,** 192–195.
14. Sweeney, H. L., Rosenfeld, S. S., Brown, F., Faust, L., Smith, J., Xing, J., Stein, L. A. & Sellers, J. R. (1998) *J. Biol. Chem.* **273,** 6262–6270.
15. Rock, R. S., Rief, M., Mehta, A. D. & Spudich, J. A. (2000) *Methods* **22,** 373–381.
16. Molloy, J. E., Burns, J. E., Kendrick-Jones, J., Tregear, R. T. & White, D. C. (1995) *Nature* **378,** 209–212.
17. Mehta, A. D., Finer, J. T. & Spudich, J. A. (1997) *Proc. Natl. Acad. Sci. USA* **94,** 7927–7931.
18. Steffen, W., Smith, D., Simmons, R. & Sleep, J. (2001) *Proc. Natl. Acad. Sci. USA* **98,** 14949–14954.
19. De La Cruz, E. M., Wells, A. L., Rosenfeld, S. S., Ostap, E. M. & Sweeney, H. L. (1999) *Proc. Natl. Acad. Sci. USA* **96,** 13726–13731.
20. Pollard, T. D. (1984) *J. Cell Biol.* **99,** 769–777.
21. Finer, J. T., Simmons, R. M. & Spudich, J. A. (1994) *Nature* **368,** 113–119.
22. Mehta, A. D., Finer, J. T. & Spudich, J. A. (1998) *Methods Enzymol.* **298,** 436–459.